CHEMISTRY OF MATERIALS
Cite This: Chem. Mater. 2019, 31, 6677−6683
Article
pubs.acs.org/cm

Morphology of Organic Semiconductors Electrically Doped from Solution Using Phosphomolybdic Acid

Tzu-Yen Huang,[†,∥] Felipe A. Larrain,[‡,∥] Carlos H. Borca,[§] Canek Fuentes-Hernandez,[‡] Hongping Yan,[†] Sebastian Alexander Schneider,[†] Wen-Fang Chou,[‡] Victor A. Rodriguez-Toro,[‡] Hans-Georg Steinrück,[†] Chuntian Cao,[†] C. David Sherrill,[*,§] Bernard Kippelen,[*,‡] and Michael F. Toney[*,†]

[†]Stanford Synchrotron Radiation Lightsource (SSRL), SLAC National Accelerator Laboratory, Menlo Park, California 94025, United States

[‡]Center for Organic Photonics and Electronics (COPE), School of Electrical and Computer Engineering, Georgia Institute of Technology, Atlanta, Georgia 30332, United States

[§]School of Chemistry and Biochemistry, Georgia Institute of Technology, Atlanta, Georgia 30332, United States

Supporting Information

ABSTRACT: The field of organic electronics aspires to enable the fabrication of low-cost, solution-processed optoelectronic devices with unique mechanical, electrical, optical, and chemical properties. Critical to the success of these aspirations is the ability to fabricate controlled doping profiles vertically or laterally (i.e., to a limited depth or area extension). However, the fabrication of stable doping profiles in polymer films has proven particularly challenging, as neither solution processing nor evaporation of dopants, such as 2,3,5,6-tetrafluoro-7,7,8,8-tetracyanoquinodimethane (F_4TCNQ), leads to vertical doping profiles due to fast diffusion on the length scale of the typical film thickness (~100 nm). This challenge was surmounted in 2017 with the first demonstration of a successful solution-based technique to fabricate doping profiles in semiconducting polymer films through immersion into a phosphomolybdic acid (PMA) solution (Kolesov et al., 2017). Still, to date, no clear picture that explains the doping phenomena has emerged. In an attempt to identify some of the key variables that govern the PMA doping process and shed light onto why this technique produces vertical doping profiles in organic films, we here report on a study of the morphology of PMA doped semiconducting polymer films, complemented theoretically with ab initio quantum chemistry calculations. We believe these results may foster the extension of the technique to other organic optoelectronic systems.

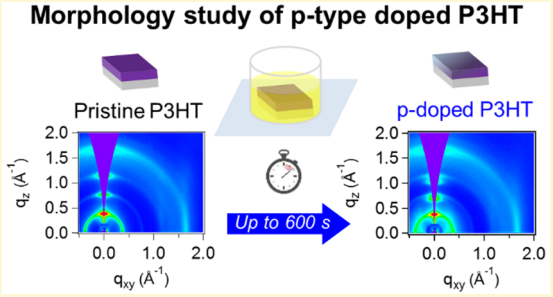

1. INTRODUCTION

Solution-based electrical doping of organic semiconductors is a widely used technique to tailor some of their physical properties (e.g., electrical conductivity and Fermi level energy), making them suitable for various optoelectronic applications.[1−4] Both n- and p-type electrical doping has been demonstrated for several semiconducting polymers, such as poly(3-hexylthiophene) (P3HT),[2,3] poly[2,6-(4,4-bis(2-ethylhexyl)-4*H*-cyclopenta[2,1-*b*;3,4-*b*′]dithiophene)-*alt*-4,7(2,1,3-benzothiadiazole)] (PCPDTBT),[5] poly[*N*,*N*′-bis(2-octyldodecyl)-1,4,5,8-napthalenedicarboximide-2,6-diyl]-*alt*-5,5′-(2,2′-bithiophene)] (P(NDIOD-T2)),[1] poly(9,9-dioctylfluorene-*alt*-*N*-(4-*s*-butylphenyl)-diphenylamine) (TFB),[3] poly(9,9-dioctylfluorene-*alt*-benzothiadiazole) (F8BT),[3] and poly(2,5-bis(3-tetradecylthiophen-2-yl)thieno-[3,2-*b*]thiophene) (PBTTT-C_{14}).[6]

Electrical doping from solution may be achieved through coating of a single film or via a process involving the sequential coating of different films. In the first approach, dopants are mixed with the semiconductor into a single solution, which is then coated onto a substrate. Alternatively, in the sequential coating approach, an undoped organic film is fabricated first, and the dopant is subsequently coated onto the semiconductor layer. A well-studied semiconductor−dopant system where both doping approaches have been explored is p-type electrical doping of P3HT using the dopant F_4TCNQ.[7,8]

Mixing of P3HT and F_4TCNQ in solution was reported to produce efficient p-type electrically doped films through an intricate interplay between dopant dissolution and charge-transfer chemistry.[9] When F_4TCNQ in the P3HT:F_4TCNQ blend is at a molar fraction larger than 0.03 (that is, 3 dopant molecules per 97 P3HT monomer units), charged complexes are formed in solution, which leads to efficient doping of P3HT. Coating this blend onto a substrate leads to P3HT films

Special Issue: Jean-Luc Bredas Festschrift

Received: March 16, 2019
Revised: May 18, 2019
Published: May 22, 2019

DOI: 10.1021/acs.chemmater.9b01069
Chem. Mater. 2019, 31, 6677−6683

with changes in their crystalline structure, compared to pristine P3HT. Specifically, the spacing between lamellae expands from 16.5 to18.5 Å, and the $\pi-\pi$ stacking diffraction peak is split into two peaks, located at 3.85 Å and 3.59 Å, respectively. These changes reveal that F_4TCNQ molecules become intercalated into ordered P3HT regions. Furthermore, doping P3HT this way drastically reduces its solubility in solution (independent of the solvent for P3HT), leading to processing difficulties, among other issues.[9]

Attempting to overcome the aforementioned issues, sequential coating of F_4TCNQ onto P3HT films was reported later, made possible by dissolving F_4TCNQ in solvents that do not dissolve the as-made P3HT film. A side-by-side comparison of the solution-mixed and sequentially processed doping of P3HT with F_4TCNQ revealed that the latter method (a) is quick, as doping takes place in less than 1 s, (b) allows for precise control of the doping level by varying the concentration of F_4TCNQ in solution, and (c) produces smoother film surfaces than those made through the solution-mixed method, essentially as smooth as pristine P3HT. Moreover, electron-diffraction spectra showed that if the solvent for F_4TCNQ does not swell P3HT crystallites, then sequential doping does not affect the P3HT $\pi-\pi$ spacing.[7] Still, it is worth noting that these ideas have recently been challenged. Recently measured electron diffraction patterns of P3HT doped with F_4TCNQ and $Mo(tfd\text{-}CO_2Me)_3$ question whether F_4TCNQ intercalates in between P3HT ordered regions. Furthermore, these data suggest that there is a decrease in $\pi-\pi$ spacing regardless of the technique used to dope the semiconducting polymer, either F_4TCNQ mixed in solution with P3HT or for sequentially doped films.[10]

While these results are relevant for single layer polymer films, most optoelectronic devices are comprised of several organic layers, each of which has a specific function. Therefore, the ability to fabricate doping profiles vertically or laterally (i.e., to a limited depth or area extension) would allow for improved performance at a reduced cost. However, the fabrication of stable doping profiles in polymer films has proven particularly challenging, as neither solution processing nor evaporation of dopants like F_4TCNQ leads to vertical doping profiles due to fast diffusion on the length scale of the typical film thickness (~100 nm). While there have been attempts to fabricate doping profiles through lamination of several layers, to the best of our knowledge there were no successful solution-based electrical doping profiles until December 2016.[11] Then, Kolesov et al. reported a successful vertical profile doping approach based on the fabrication of the semiconductor film followed by its immersion into a phosphomolybdic acid (PMA) solution using a proper solvent.[7] Using this method, it was shown that doped organic films with increased electrical conductivity and work function, reduced solubility in the processing solvent, and improved photo-oxidative stability in air could be realized. Furthermore, since the doping was limited in depth into the film, the combination with amine-containing polymers enabled the first demonstration of a single layer organic solar cell.[12]

Thereafter, Larrain et al. optimized this technique by increasing its stability in air.[13] Through replacing nitromethane as the processing solvent with acetonitrile, the PMA−solvent blend showed increased stability in air without losing its doping ability. Additionally, organic solar cells fabricated using the updated approach also showed improved stability when exposed to air. It is important to note that other methods to fabricate controlled doping profiles via electrical fields have recently been reported.[14]

Still, from a molecular perspective, the interplay between P3HT and PMA molecules that leads to p-type electrical doping of the organic layer remains unclear. In other words, what are the key variables that govern this process, and ultimately why does this technique produce vertical doping profiles? To answer these questions, herein we report on a study of the morphology of PMA-doped P3HT films using grazing-incidence wide-angle X-ray scattering (GIWAXS). By varying the immersion time of P3HT layers into the PMA solution, we evaluate how morphological changes related to PMA doping evolve as a function of immersion time. Then, we designed and conducted ab initio quantum chemistry calculations to shed light onto the intermolecular interactions between the dopant and P3HT that could lead to stable and doped semiconducting films. We believe these results represent a step forward on the path to unraveling the doping mechanism, which in turn would enable to tailor the profile and penetration depth of p-type dopants into organic layers.

2. METHODS

2.1. Materials. Poly(3-hexylthiophene) (P3HT, 4002-E) was purchased from Rieke Metals. 12-Molybdophosphoric acid hydrate (PMA, Mw = 1825.25 g mol^{-1}) was purchased from Alfa Aesar. Acetonitrile (anhydrous, 99.8% purity) and chlorobenzene (anhydrous, 99.8% purity) were purchased from Sigma-Aldrich. All chemicals were used as received without further purification.

2.2. Preparation of P3HT and PMA-Doped P3HT Films. Silicon wafers were cleaved into 1 in. × 1 in. pieces and used as substrates for P3HT semiconducting films. The substrates were solvent cleaned in sequential ultrasonic baths of Liquinox detergent in distilled water, distilled water, acetone, and 2-propanol, each lasting 40 min and at a temperature of 40 °C, and blown dry with N_2. Subsequently, the samples were transferred into a N_2-filled glovebox.

P3HT was weighed on an electronic scale in air and added to an amber glass vial with a magnetic stirrer. The vial was transferred to a N_2-filled glovebox where the P3HT was dissolved to a concentration of 10 mg mL^{-1} using chlorobenzene and stirred overnight at room temperature. The P3HT solution was filtered using a 0.2-μm-pore PTFE filter and spin coated onto silicon wafers at a speed of 800 rpm, with an acceleration of 10 000 rpm s^{-1} for 30 s. Subsequently, samples were left in glass Petri dishes to solvent anneal for 1 h and thermally anneal on a hot plate at 150 °C for 10 min. The as-made 30 nm-thick P3HT films were dipped into a 0.5 M solution of PMA in acetonitrile for 10, 60, and 600 s and then thoroughly rinsed with pure acetonitrile to remove PMA residues.

2.3. Grazing-Incidence Wide-Angle X-ray Scattering (GIWAXS) Measurement. GIWAXS was measured at the Stanford Synchrotron Radiation Lightsource (SSRL) beamline 11-3 in a helium-filled chamber, with an X-ray wavelength of 0.9752 Å and sample to detector distance of 25 cm, at an incident angle of 0.12°. The spectra were recorded on a 2D X-ray detector (MX225, Rayonix LLC) with a pixel size of 73 μm (3072 × 3072 pixels) and analyzed using the Nika and WAXStools package for Igor software (WaveMetrics, Inc.).[15,16] In this work, the polar angle (χ) is defined as the angle of the observed diffraction from the normal to the substrate. Thus, $\chi = 0°$ is perpendicular to the substrate and $\chi = 90°$ is parallel to the substrate. The out-of-plane sector is considered at 0−20°, and the in-plane sector is 70−90°.

2.4. Quantum Chemistry Calculations. Ab initio calculations were executed in two stages: geometry optimization of monomers and potential energy surface (PES) scan using rigid monomers. All calculations were carried out using the computational chemistry package Psi4 version 1.3a1.[17]

In the first stage, the structure of each molecule, molybdenum trioxide and thiophene, was optimized separately employing density-

DOI: 10.1021/acs.chemmater.9b01069
Chem. Mater. 2019, 31, 6677−6683

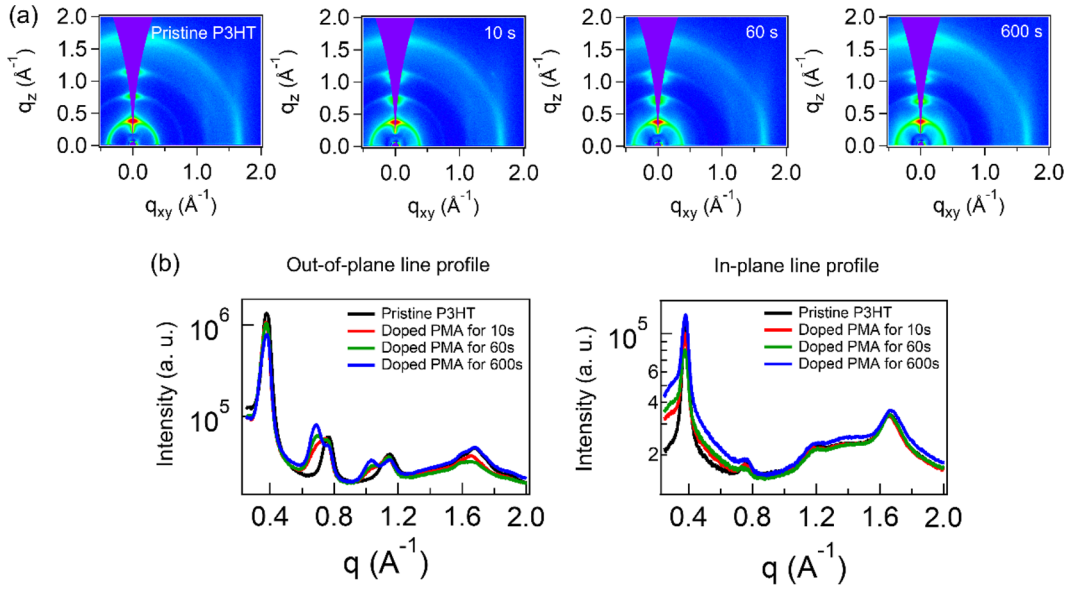

Figure 1. (a) 2-D GIWAXS patterns of pristine P3HT and PMA doped P3HT, where film immersion time in 0.5 M PMA solution in acetonitrile was varied as 10 s, 60 s, and 600 s. (b) Out-of-plane and in-plane line profiles for pristine and PMA doped P3HT.

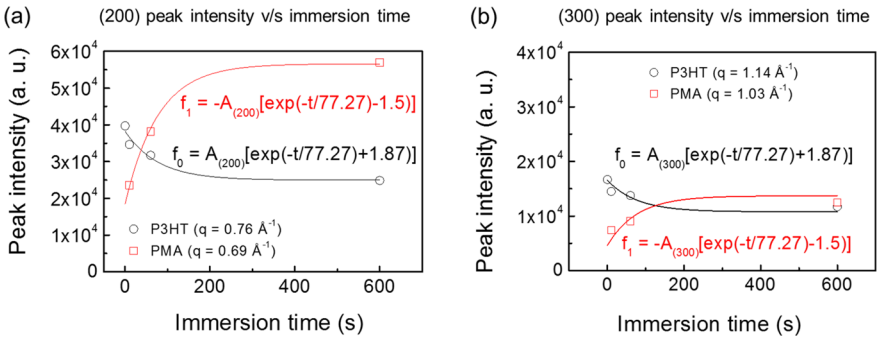

Figure 2. (a) Intensity of the (200) diffraction peaks corresponding to pristine P3HT and PMA. (b) Intensity of the (300) diffraction peaks corresponding to pristine P3HT and PMA. Profiles are fitted to an exponential decay function.

fitted second order Møller−Plesset perturbation theory (DF-MP2).[18,19] The def2-QZVPPD basis set and its corresponding effective-core potential (ECP) for molybdenum were used in these geometry optimizations.[20] The basis projection technique was utilized to facilitate the convergence of the self-consistent field procedure, using the smaller def2-SVP basis set as the initial guess for the larger def2-QZVPPD. Both basis sets share the same ECP for molybdenum.

Once the optimized geometry of each molecule was obtained, dimers and trimers in three different conformations were constructed. The first dimer conformation, denoted as *T-shape*, contains a molecule of thiophene with its sulfur atom pointing at the molybdenum atom of the trioxide, which is placed on a perpendicular plane to that of the thiophene. The *stacked* dimer conformation is formed by placing both molecules on parallel planes aligned by their center of mass. The *coplanar* dimer conformation has both molecules placed on the same plane with the sulfur of thiophene pointing toward the molybdenum atom of the trioxide.

Then, trimer conformations were built by placing an additional molecule of thiophene on each of the previously described dimers. The *T-shape trimer* contained another molecule of thiophene with its sulfur atom pointing at the molybdenum atom of the perpendicularly placed trioxide but in the opposite direction to the other thiophene. The *stacked trimer* is essentially a sandwich, with the molybdenum trioxide in the middle. Finally, the *coplanar trimer* has an additional thiophene with its sulfur atom pointing toward the molybdenum, in the opposite direction from the other thiophene.

The second stage involved the computation of PES for each of these dimer and trimer structures. In the PESs, the molecules are separated from each other, while keeping their internal geometries unmodified. The interaction energy is computed at each displacement, correcting for the basis set superposition error using the Boys−Bernardi counterpoise correction.[21] The translation coordinate in T-shape and coplanar configurations is given by the distance of separation between the sulfur and the molybdenum atoms. In the stacked configuration, it is given by the interplanar separation. Our calculations account for electrostatic effects as a result of charge transfer.

3. RESULTS AND DISCUSSION

The study began by evaluating how morphological changes in PMA doped semiconducting polymer films progress as a function of immersion time. This was determined by varying the immersion time of P3HT layers into PMA solution and characterizing the morphology of the resulting doped films using GIWAXS.

Figure 1a shows the 2-D GIWAXS pattern of pristine and PMA doped P3HT films for 10, 60, and 600 s, while Figure 1b highlights the out-of-plane (OOP) and in-plane (IP) line profiles for each condition. Per the out-of-plane line profile, the pristine P3HT film features the expected (100), (200), and (300) diffraction peaks at q = 0.38 Å^{-1}, 0.76 Å^{-1}, and 1.14 Å^{-1}

DOI: 10.1021/acs.chemmater.9b01069
Chem. Mater. 2019, 31, 6677−6683

and a broad $\pi-\pi$ stacking peak at q = 1.66 Å^{-1} with broad polar angle distribution, comprising both edge-on and face-on orientation with respect to the Si substrate. The broad (in polar angle) $\pi-\pi$ stacking peak is attributed to the coexistence of both face-on and edge-on molecular packing orientation in the film, consistent with the literature.[22]

As the P3HT film is doped by immersion in a 0.5 M solution of PMA in acetonitrile for 10 s (Figure 1b), the (200) diffraction peak splits into two peaks at q = 0.69 Å^{-1} and 0.76 Å^{-1}. The peak at 0.76 Å^{-1} corresponds to pristine P3HT, whereas the new peak at 0.69 Å^{-1} is associated with the PMA molecule modifying the P3HT packing. The (300) diffraction signal also splits into two peaks, one at q = 1.03 Å^{-1} and another at 1.14 Å^{-1}. Similarly, the peak at 1.14 Å^{-1} corresponds to neat P3HT while the new peak at 1.03 Å^{-1} relates to PMA-modified P3HT packing. From these data, it is clear that PMA becomes intercalated with P3HT lamellae. The lamellae d-spacing increases due to the intercalation. In contrast, the $\pi-\pi$ stacking peak does not shift in position.

Further increasing the doping time to 60 and 600 s correlates with peak intensity increases for the (100), (200), and (300) diffraction peaks, while their q position remains unchanged. A decreased intensity for neat P3HT peaks along with higher scattering intensity from PMA peaks suggests that more PMA intercalates into P3HT lamellae with longer immersion times. Figure 2 highlights these changes by comparing the intensity of the (200) and (300) diffraction peaks corresponding to neat P3HT and PMA-modified packing (calculation procedure reported earlier[16]). The results are in good agreement with an exponential function fit which suggests that changes in peak intensity would be negligible after 200 s, in line with the self-limiting nature of the phenomena observed in our previous work.[12]

While OOP line profiles of PMA doped P3HT exhibit distinctive peaks corresponding to neat P3HT and PMA molecules for the (200) and (300) diffraction, the (100) diffraction does not clearly split for any immersion time (Figure S2), although the shape changes with a tail developing toward smaller q-values. This suggests that the neat P3HT peak from the (100) diffraction is overlapping with the signal corresponding to PMA-modified P3HT packing, but additional 2-D GIWAXS patterns with various X-ray incident angles are required to confirm this claim (current incident angle is 0.12°). Varying this angle would also provide a broad picture of the distribution of PMA molecules into the doped film, as it would help with characterizing regions closer to the surface or deeper into the sample. Thus, the X-ray incidence angle was varied to 0.04°, 0.08°, 0.16°, and 0.20° on the P3HT film immersed into PMA solution for 600 s. This sample was selected as its previous GIWAXS characterization (per Figure 1b) suggests it contains the largest amount of PMA molecules compared to all other samples immersed for shorter times. The corresponding 2-D GIWAXS patterns and OOP line profiles are depicted in Figure S3 and Figure 3a, respectively.

With an X-ray incident angle of 0.04°, the (100) diffraction does split into two distinctive peaks as shown in Figure 3a (zoomed in Figure S4a), which indicates that the neat P3HT and PMA molecules do overlap in the OOP profile taken at an X-ray incidence of 0.12°. Moreover, the intensities of both the neat P3HT and the PMA-modified peaks change with the angle of incidence. Figure 3b plots the ratio between the area of the PMA peak and the neat P3HT peak (calculation procedure reported earlier[16]). These data show that PMA

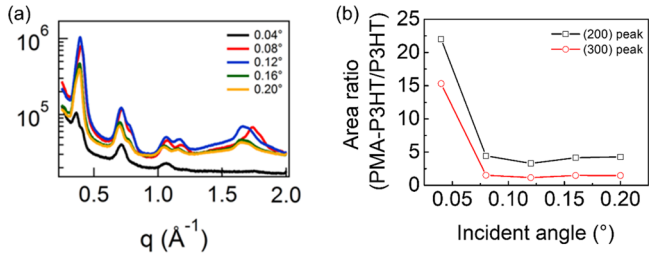

Figure 3. (a) Out-of-plane line profile from GIWAXS patterns taken at various incident angles in a P3HT sample immersed into PMA solution for 600 s. (b) Ratio of PMA to neat P3HT signals for diffractions (200) and (300) as a function of incidence angle.

molecules penetrate only down to a limited depth of the P3HT film and dopant molecules concentrate close to the surface of the sample, which is consistent with previous characterizations of the distribution of dopants into the depth of the layer. While the evidence clearly indicates that the P3HT crystal is altered by PMA molecules, it does not provide any insight into whether PMA molecules exist in the amorphous regions of the film.

From a molecular perspective, it remains unclear what constitutes the interplay between P3HT, solvent, and PMA molecules that leads to stable vertical doping profiles within the organic layer. Furthermore, the self-limiting nature of PMA doping distinguishes the technique from all other solution-based electrical doping methods. Thus, to unravel its cause(s) is key to further tailor the profile and penetration depth of dopants into organic layers (e.g., by using other polyoxometalates), broadening its applicability to other organic optoelectronic systems (e.g., those with several organic layers thinner than 60 nm).

Careful examination of previous experimental data suggests an interaction between the sulfur atom in the thiophene of P3HT and the molybdenum atom of PMA. X-ray photoelectron spectroscopy (XPS) results suggested the reduction of Mo(3d) alongside with the oxidation of S(2s) in PMA-im-P3HT films, compared to neat P3HT, which would be also evidence of an electron-transfer reaction between the two compounds. Furthermore, increased photo-oxidation stability of PMA-im-P3HT films as compared to pristine ones also points out to molecular hindrance of the photo-oxidation mechanism that is initiated on the alkyl side chain and leads to sulfur oxidation (S═O) on the backbone of P3HT.[12,23] Following this line of thought, we set out to complement the morphological characterization by studying the interaction between sulfur and molybdenum. To do so, we designed and conducted ab initio quantum chemistry calculations dealing directly with the intermolecular interactions between the dopant and P3HT, in an effort to provide insights related to the self-limiting nature of the doping method.

On the one hand, according to stoichiometry, there are 12 units of molybdenum trioxide (MoO_3) per PMA molecule; therefore, the MoO_3 can be thought of as a subunit of the dopant. On the other hand, thiophene is the main chemical feature in each monomer of the P3HT polymer. Therefore, model systems consisting of molybdenum trioxide and thiophene molecules were studied using ab initio methods. Dimers and trimers involving the thiophene and either one or two molybdenum trioxide molecules were constructed and studied in three conformations by calculating their interaction energy as a function of separation, as described in detail in the

DOI: 10.1021/acs.chemmater.9b01069
Chem. Mater. 2019, 31, 6677−6683

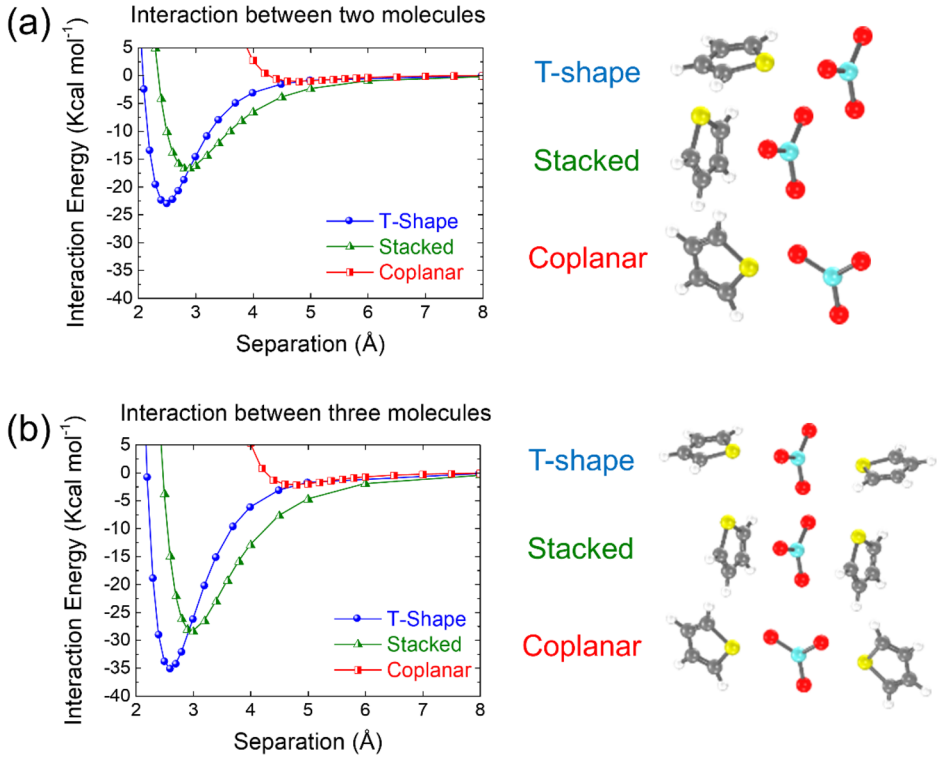

Figure 4. (a) Thiophene−MoO_3 interaction energy as a function of distance between S and Mo atoms. (b) Thiophene−MoO_3−thiophene interaction energy as a function of interplanar separation.

Methods section. Interaction energies as a function of separation for each system and conformation are plotted in Figure 4, from which valuable insights are obtained.

Our GIWAXS data determined the $\pi-\pi$ stacking distance of P3HT crystals to be 3.7 Å. Thus, since the optimal geometry of a PMA molecule measures 1 nm in diameter, it is unlikely that the entire molecule would fit in between two polymer backbones. But what if the PMA molecules break up into smaller MoO_3 molecules and then reach the crystalline phases of P3HT? Calculations of interaction energies as presented in Figure 4 confirm that, even if that is the case, it would be energetically too costly for them to distort the $\pi-\pi$ stacking.

Indeed, as it can be read from Figure 4, in the region of the interaction energy curve that describes the scenario where a dopant molecule would fit in between the $\pi-\pi$ stacking (*stacked* conformers at separation distances below 3.7/2 = 1.85 Å), the curves exhibit a highly repulsive interaction (i.e., positive value of interaction energy). In other words, this scenario is unlikely unless the dopant is forcefully introduced in the stack. These results agree with all GIWAXS measurements on PMA doped films, where no significant distortion of the $\pi-\pi$ stacking is observed.

Moreover, both the *T-shape* and *stacked* conformations exhibit attractive interaction energies in the trimer system, up to ∼1/4 of the energy of a carbon−carbon covalent bond at room temperature (83−90 kcal mol^{-1} at 298 K). These data suggest that once PMA molecules become intercalated between P3HT lamellae, they fall into a potential well and probably stay there. This feature directly supports the self-limiting nature of the PMA doping phenomena observed experimentally and clearly distinguishes the process from mere diffusion of dopant molecules into the film, as is typically the case with most solution-based doping techniques of organic semiconductors. However, our calculations do not explain how the dopant penetrates into the film in the first place. In fact, it remains unclear why PMA molecules stay near the surface of P3HT layers while F_4TCNQ penetrates the full volume when sequentially doped from solution in acetonitrile. We speculate that F_4TCNQ might fit more easily into the amorphous domains of acetonitrile-swollen P3HT, compared to the bulkier PMA molecule. Indeed, the PMA anion, containing a phosphate moiety attached to 12 molybdenum trioxide subunits, has a total diameter of 10.2 ± 0.5 Å. Furthermore, while acetonitrile is not a good solvent for P3HT, it has been shown that it swells it to a limited extent.[24]

4. CONCLUSIONS

To identify some of the key driving forces that govern the PMA doping phenomena and shed light onto why this technique produces vertical doping profiles in organic films, the morphology of PMA doped semiconducting polymer films was investigated experimentally (using GIWAXS measurements) and theoretically (through ab initio quantum chemistry calculations).

First, the data confirm that organic film immersion time, for a given crystallinity level and PMA solution concentration, has a direct impact on the amount of PMA molecules that settle in between the lamellae. However, immersion time does not change the place where dopants locate within the film. While doping level progresses with immersion time, it is likely that most dopants penetrate the film well before 10 s, probably in a much shorter time scale. Furthermore, the process appears to saturate after a few minutes of immersion time, in line with previous findings.[12]

Our ab initio quantum chemistry calculations directly support the self-limiting nature of the PMA doping phenomena (as observed experimentally) and clearly distin-

DOI: 10.1021/acs.chemmater.9b01069
Chem. Mater. 2019, 31, 6677−6683

guish the process from a mere diffusion driven one. We speculate that vertical doping profiles appear due to interactions between PMA molecules and P3HT lamellae, as dopants reaching this region may very likely fall into a potential well.

■ ASSOCIATED CONTENT

Supporting Information

The Supporting Information is available free of charge on the ACS Publications website at DOI: 10.1021/acs.chemmater.9b01069.

Details of various GIWAXS data and analysis as well as molecular structures, including four figures (PDF)

■ AUTHOR INFORMATION

Corresponding Authors

*(B.K.) E-mail: bernard.kippelen@ece.gatech.edu.
*(C.D.S.) E-mail: sherrill@gatech.edu.
*(M.F.T.) E-mail: mftoney@slac.stanford.edu.

ORCID

Carlos H. Borca: 0000-0003-0683-7613
Canek Fuentes-Hernandez: 0000-0001-7958-3699
Hans-Georg Steinrück: 0000-0001-6373-0877
C. David Sherrill: 0000-0002-5570-7666
Michael F. Toney: 0000-0002-7513-1166

Author Contributions

‖T.-Y.H. and F.A.L. contributed equally.

Notes

The authors declare no competing financial interest.

■ ACKNOWLEDGMENTS

This work was supported by the Department of the Navy, Office of Naval Research Award Nos. N00014-14-1-0580, N00014-16-1-2520, and N00014-16-1-2678. Use of Stanford Synchrotron Radiation Lightsource, SLAC National Accelerator Laboratory, is supported by the U.S. Department of Energy, Office of Science, Office of Basic Energy Sciences, under Contract No. DE-AC02-76SF00515. Part of this work was performed at the Stanford Nano Shared Facilities (SNSF), supported by the National Science Foundation under award ECCS-1542152. T.-Y.H. acknowledges the support of Ministry of Science and Technology (MOST), Taiwan, though the Overseas Project for Postdoctoral Research Abroad Program (PRAP) (105-2917-I-564-044). C.D.S. gratefully acknowledges support from the National Science Foundation under Award CHE-1566192. We also acknowledge the support of CONICYT (Chilean National Commission for Scientific and Technological Research) through the Doctoral Fellowship program "Becas Chile", Grant No. 72150387 for F. A. L., as well as support from COLCIENCIAS (Colombian Administrative Department of Science, Technology and Innovation) through the program Fulbright-Colciencias for V. A. R.-T. Furthermore, we acknowledge the use of research cyberinfrastructure resources and services provided by the Partnership for an Advanced Computing Environment (PACE) at the Georgia Institute of Technology.

■ REFERENCES

(1) Schlitz, R. A.; Brunetti, F. G.; Glaudell, A. M.; Miller, P. L.; Brady, M. A.; Takacs, C. J.; Hawker, C. J.; Chabinyc, M. L. Solubility-limited extrinsic n-type doping of a high electron mobility polymer for thermoelectric applications. *Adv. Mater.* **2014**, *26* (18), 2825−30.
(2) Sun, J.; Yeh, M. L.; Jung, B. J.; Zhang, B.; Feser, J.; Majumdar, A.; Katz, H. E. Simultaneous Increase in Seebeck Coefficient and Conductivity in a Doped Poly(alkylthiophene) Blend with Defined Density of States. *Macromolecules* **2010**, *43* (6), 2897−2903.
(3) Yim, K.-H.; Whiting, G. L.; Murphy, C. E.; Halls, J. J. M.; Burroughes, J. H.; Friend, R. H.; Kim, J.-S. Controlling Electrical Properties of Conjugated Polymers via a Solution-Based p-Type Doping. *Adv. Mater.* **2008**, *20* (17), 3319−3324.
(4) Salzmann, I.; Heimel, G.; Oehzelt, M.; Winkler, S.; Koch, N. Molecular Electrical Doping of Organic Semiconductors: Fundamental Mechanisms and Emerging Dopant Design Rules. *Acc. Chem. Res.* **2016**, *49* (3), 370−8.
(5) Deschler, F.; Da Como, E.; Limmer, T.; Tautz, R.; Godde, T.; Bayer, M.; von Hauff, E.; Yilmaz, S.; Allard, S.; Scherf, U.; Feldmann, J. Reduced charge transfer exciton recombination in organic semiconductor heterojunctions by molecular doping. *Phys. Rev. Lett.* **2011**, *107* (12), 127402.
(6) Cochran, J. E.; Junk, M. J. N.; Glaudell, A. M.; Miller, P. L.; Cowart, J. S.; Toney, M. F.; Hawker, C. J.; Chmelka, B. F.; Chabinyc, M. L. Molecular Interactions and Ordering in Electrically Doped Polymers: Blends of PBTTT and F4TCNQ. *Macromolecules* **2014**, *47* (19), 6836−6846.
(7) Jacobs, I. E.; Aasen, E. W.; Oliveira, J. L.; Fonseca, T. N.; Roehling, J. D.; Li, J.; Zhang, G.; Augustine, M. P.; Mascal, M.; Moulé, A. J. Comparison of solution-mixed and sequentially processed P3HT:F4TCNQ films: effect of doping-induced aggregation on film morphology. *J. Mater. Chem. C* **2016**, *4* (16), 3454−3466.
(8) Méndez, H.; Heimel, G.; Winkler, S.; Frisch, J.; Opitz, A.; Sauer, K.; Wegner, B.; Oehzelt, M.; Röthel, C.; Duhm, S.; Többens, D.; Koch, N.; Salzmann, I. Charge-transfer crystallites as molecular electrical dopants. *Nat. Commun.* **2015**, *6*, 8560.
(9) Duong, D. T.; Wang, C.; Antono, E.; Toney, M. F.; Salleo, A. The chemical and structural origin of efficient p-type doping in P3HT. *Org. Electron.* **2013**, *14* (5), 1330−1336.
(10) Liu, W.; Müller, L.; Ma, S.; Barlow, S.; Marder, S. R.; Kowalsky, W.; Köhn, A.; Lovrincic, R. Origin of the $\pi-\pi$ Spacing Change upon Doping of Semiconducting Polymers. *J. Phys. Chem. C* **2018**, *122* (49), 27983−27990.
(11) Jacobs, I. E.; Moule, A. J. Controlling Molecular Doping in Organic Semiconductors. *Adv. Mater.* **2017**, *29* (42), 1703063.
(12) Kolesov, V. A.; Fuentes-Hernandez, C.; Chou, W. F.; Aizawa, N.; Larrain, F. A.; Wang, M.; Perrotta, A.; Choi, S.; Graham, S.; Bazan, G. C.; Nguyen, T. Q.; Marder, S. R.; Kippelen, B. Solution-based electrical doping of semiconducting polymer films over a limited depth. *Nat. Mater.* **2017**, *16* (4), 474−480.
(13) Larrain, F. A.; Fuentes-Hernandez, C.; Chou, W.-F.; Rodriguez-Toro, V. A.; Huang, T.-Y.; Toney, M. F.; Kippelen, B. Stable solvent for solution-based electrical doping of semiconducting polymer films and its application to organic solar cells. *Energy Environ. Sci.* **2018**, *11* (8), 2216−2224.
(14) Muller, L.; Rhim, S. Y.; Sivanesan, V.; Wang, D.; Hietzschold, S.; Reiser, P.; Mankel, E.; Beck, S.; Barlow, S.; Marder, S. R.; Pucci, A.; Kowalsky, W.; Lovrincic, R. Electric-Field-Controlled Dopant Distribution in Organic Semiconductors. *Adv. Mater.* **2017**, *29* (30), 1701466.
(15) Ilavsky, J. Nika: software for two-dimensional data reduction. *J. Appl. Crystallogr.* **2012**, *45* (2), 324−328.
(16) Oosterhout, S. D.; Savikhin, V.; Zhang, J.; Zhang, Y.; Burgers, M. A.; Marder, S. R.; Bazan, G. C.; Toney, M. F. Mixing Behavior in Small Molecule:Fullerene Organic Photovoltaics. *Chem. Mater.* **2017**, *29* (7), 3062−3069.
(17) Parrish, R. M.; Burns, L. A.; Smith, D. G. A.; Simmonett, A. C.; DePrince, A. E., 3rd; Hohenstein, E. G.; Bozkaya, U.; Sokolov, A. Y.; Di Remigio, R.; Richard, R. M.; Gonthier, J. F.; James, A. M.; McAlexander, H. R.; Kumar, A.; Saitow, M.; Wang, X.; Pritchard, B. P.; Verma, P.; Schaefer, H. F., 3rd; Patkowski, K.; King, R. A.; Valeev, E. F.; Evangelista, F. A.; Turney, J. M.; Crawford, T. D.; Sherrill, C. D.

DOI: 10.1021/acs.chemmater.9b01069
Chem. Mater. 2019, 31, 6677−6683

Psi4 1.1: An Open-Source Electronic Structure Program Emphasizing Automation, Advanced Libraries, and Interoperability. *J. Chem. Theory Comput.* **2017**, *13* (7), 3185−3197.
(18) Feyereisen, M.; Fitzgerald, G.; Komornicki, A. Use of approximate integrals in ab initio theory. An application in MP2 energy calculations. *Chem. Phys. Lett.* **1993**, *208* (5), 359.
(19) Bernholdt, D. E.; Harrison, R. J. Large-scale correlated electronic structure calculations: the RI-MP2 method on parallel computers. *Chem. Phys. Lett.* **1996**, *250*, 8.
(20) Weigend, F.; Ahlrichs, R. Balanced basis sets of split valence, triple zeta valence and quadruple zeta valence quality for H to Rn: Design and assessment of accuracy. *Phys. Chem. Chem. Phys.* **2005**, *7* (18), 3297−305.
(21) Boys, S.F.; Bernardi, F. The calculation of small molecular interactions by the differences of separate total energies. Some procedures with reduced errors. *Mol. Phys.* **1970**, *19* (4), 553.
(22) Sirringhaus, H.; Brown, P. J.; Friend, R. H.; Nielsen, M. M.; Bechgaard, K.; Langeveld-Voss, B. M. W.; Spiering, A. J. H.; Janssen, R. A. J.; Meijer, E. W.; Herwig, P.; de Leeuw, D. M. Two-dimensional charge transport in self-organized, high-mobility conjugated polymers. *Nature* **1999**, *401*, 685.
(23) Sai, N.; Leung, K.; Zador, J.; Henkelman, G. First principles study of photo-oxidation degradation mechanisms in P3HT for organic solar cells. *Phys. Chem. Chem. Phys.* **2014**, *16* (17), 8092−9.
(24) Murrey, T. L.; Guo, K.; Mulvey, J. T.; Lee, O. A.; Cendra, C.; Bedolla-Valdez, Z. I.; Salleo, A.; Moulin, J.-F.; Hong, K.; Moulé, A. J. Additive solution deposition of multi-layered semiconducting polymer films for design of sophisticated device architectures. *J. Mater. Chem. C* **2019**, *7* (4), 953−960.

DOI: 10.1021/acs.chemmater.9b01069
Chem. Mater. 2019, 31, 6677−6683